AGU PUBLICATIONS

Geophysical Research Letters

RESEARCH LETTER
10.1002/2017GL073855

Key Points:
- Medium-scale thermospheric GWs in bottomside *F* region show similar longitudinal distribution as equatorial plasma bubbles
- Thermosphere GWs show opposite seasonal variation to that of equatorial plasma bubbles
- Thermospheric GWs in the tropics are likely secondary waves generated by deep convection

Correspondence to:
H. Liu,
huixin@serc.kyushu-u.ac.jp

Citation:
Liu, H., N. Pedatella, and K. Hocke (2017), Medium-scale gravity wave activity in the bottomside *F* region in tropical regions, *Geophys. Res. Lett.*, *44*, 7099–7105, doi:10.1002/2017GL073855.

Received 18 MAY 2017
Accepted 22 JUN 2017
Accepted article online 26 JUN 2017
Published online 17 JUL 2017

Medium-scale gravity wave activity in the bottomside *F* region in tropical regions

Huixin Liu[1], Nicholas Pedatella[2], and Klemens Hocke[3]

[1]Department of Earth and Planetary Science, Kyushu University, Fukuoka, Japan, [2]High Altitude Observatory, National Center for Atmospheric Research, Boulder, Colorado, USA, [3]Institute of Applied Physics, University of Bern, Bern, Switzerland

Abstract Thermospheric gravity waves (GWs) in the bottomside *F* region have been proposed to play a key role in the generation of equatorial plasma bubbles (EPBs). However, direct observations of such waves are scarce. This study provides a systematic survey of medium-scale (<620 km) neutral atmosphere perturbations at this critical altitude in the tropics, using 4 years of in situ Gravity Field and Steady-State Ocean Circulation Explorer satellite measurements of thermospheric density and zonal wind. The analysis reveals pronounced features on their global distribution and seasonal variability: (1) A prominent three-peak longitudinal structure exists in all seasons, with stronger perturbations over continents than over oceans. (2) Their seasonal variation consists of a primary semiannual oscillations (SAO) and a secondary annual oscillation (AO). The SAO component maximizes around solstices and minimizes around equinoxes, while the AO component maximizes around June solstice. These GW features resemble those of EPBs in spatial distribution but show opposite trend in climatological variations. This may imply that stronger medium-scale GW activity does not always lead to more EPBs. Possible origins of the bottomside GWs are discussed, among which tropical deep convection appears to be most plausible.

1. Introduction

A unique phenomenon in the evening sector is the occurrence of equatorial spread *F* (ESF), also called equatorial plasma bubbles (EPB), which has received intensive attention because of its complex physics and severe influence on communication and navigation [e.g., *Watanabe and Oya*, 1986; *Burke et al.*, 2004; *Abdu et al.*, 2009; *Yokoyama et al.*, 2015, and references therein]. Among various aspects involved with the occurrence of EPBs, seeding is the least understood. Medium-scale gravity waves (GWs) with horizontal scales of a few hundred kilometers in the bottomside *F* region have been frequently suggested to play a key role in EPB seeding [e.g., *Fritts et al.*, 2008; *Abdu et al.*, 2009]. However, there are also a body of studies that argue against this hypothesis [e.g., *Kudeki et al.*, 2007; *Yokoyama et al.*, 2015]. The lack of direct measurements of gravity waves at this critical altitude undoubtedly contributes to this debate. The GW activity near sunset in the bottomside has been so far mainly inferred from plasma measurements made by digisondes or medium frequency radars.

In this study, we carry out a systematic survey of medium-scale thermospheric gravity waves in the bottomside *F* region using 4 years of in situ neutral density and zonal wind measurements from the Gravity Field and Steady-State Ocean Circulation Explorer (GOCE) [*Rebhan et al.*, 2000]. GOCE was a Sun-synchronous satellite flying in a near-circular orbit around 250 km altitude, with an inclination of 96.7° in the dawn-dusk meridional plane (7–19 LT). The mission was from 17 March 2009 to 11 November 2013. The Sun-synchronous nature gives GOCE a great advantage over many other satellites (e.g., CHAMP) in studying the evening sector by providing a large amount of measurements that vary little in local time. This enables a clean separation in seasons with ample sampling without contamination from local time drift (a common problem faced by non-Sun-synchronous satellites). The climatology of the zonal wind obtained from GOCE has been reported in *Liu et al.* [2016], showing a strong eastward wind jet along the dip equator in the evening sector.

2. Data

Thermospheric density and wind were derived from GOCE measurements at a 10 s sampling cadence [*Doornbos et al.*, 2013], corresponding to about 77.5 km along-track distance. The following analysis uses quiet

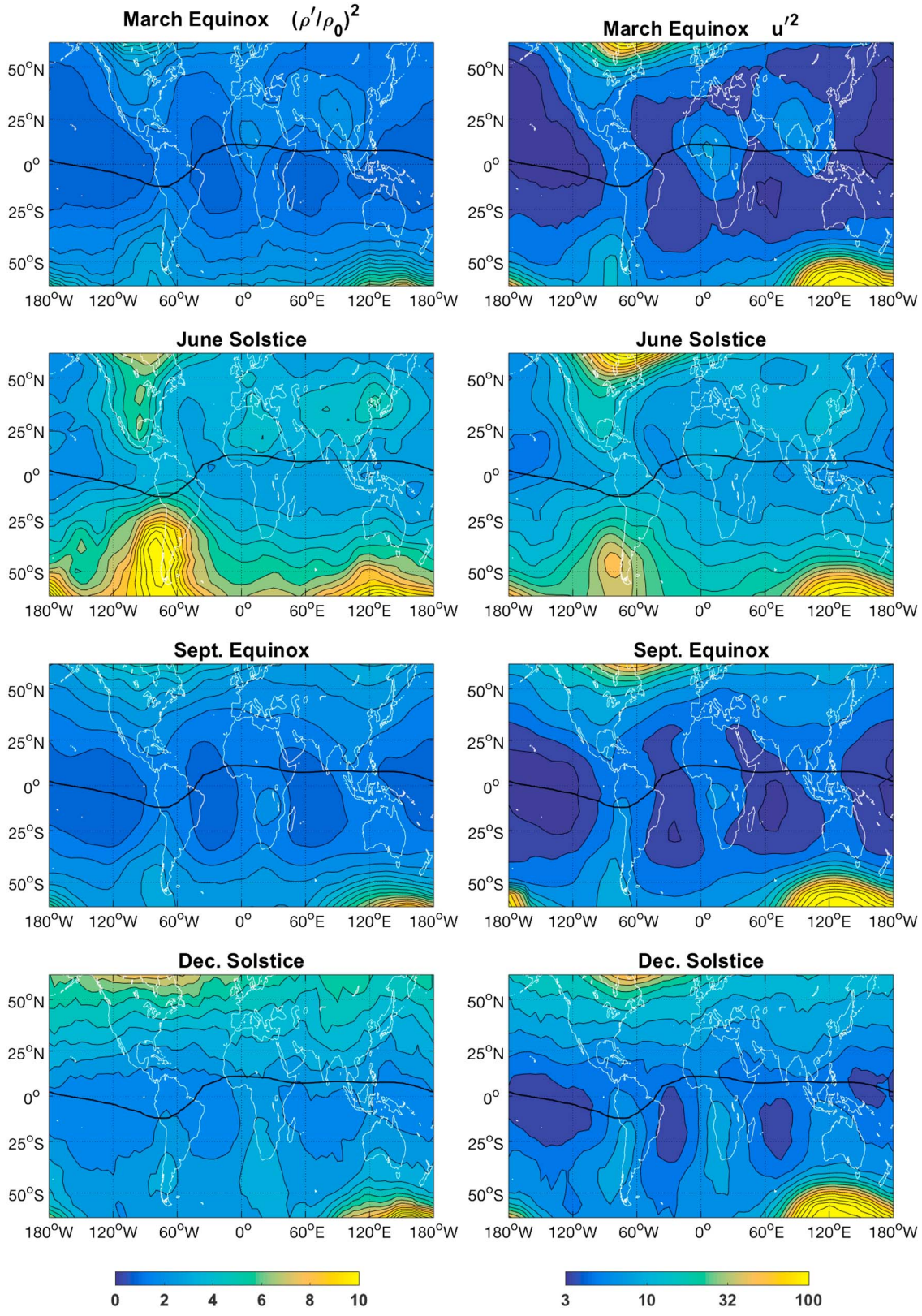

Figure 1. Global distribution of gravity waves between [60°S, 60°N] at ~250 km altitude averaged over years 2010–2013. (left column) GW activity derived from the density, in unit of 10^{-5}; (right column) GW activity derived from the zonal wind, in unit of m^2/s^2. March equinox covers March–May, June solstice covers June–August, Sept. Equinox covers September–November, and Dec. Solstice covers December–February. The average $F_{10.7}$ index is about 110 sfu. The thick black line marks the dip equator.

time data ($Kp < 3$) during 1 January 2010 to 20 October 2013 near the dusk terminator (1820–1920 LT). The orbit height varied from 220 to 280 km, with an average around ~250 km. The solar flux varied from low ($F_{10.7} \approx 65$ solar flux units (sfu)) to medium ($F_{10.7} \approx 175$ sfu) levels [*Liu et al.*, 2016, Figure 1].

To extract medium-scale gravity wave activities with a few hundred kilometer horizontal scales, we apply a similar method as that of *Park et al.* [2014]. Briefly, a mean background latitudinal profile of the density (ρ_0) and wind (u_0) with scales larger than 620 km is obtained by applying a low-pass filter to the measurements along the satellite track. Perturbations (ρ', u') are then obtained by subtracting ρ_0 and u_0 from ρ and u. This is a widely used procedure and effectively extracts gravity waves with scale lengths between about 155 – 620 km along satellite tracks.

In describing GW wave activities, *Park et al.* [2014] used the mean of the absolute values of normalized density perturbation, while *Forbes et al.* [2016] used the root-mean-square of the density difference. Here in this study, we choose to follow the conventions of gravity wave studies and take the variance of these perturbations, that is, $\left(\frac{\rho'}{\rho_0}\right)^2$ and u'^2, as the parameters to represent wave activity [e.g., *Hocke and Tsuda*, 2001; *Hei et al.*, 2008; *Jacobi*, 2014]. The quantity, $\left(\frac{\rho'}{\rho_0}\right)^2$, is proportional to the wave potential energy, when assuming the density perturbation is directly linked to the temperature perturbation. The quantity, u'^2, is proportional to the kinetic part of the wave energy [*Hei et al.*, 2008]. We bin these two quantities into 5°×5° geographic longitude×latitude grids for each month during the observational period and take their median values as a robust estimate of the GW activity in each grid. A three-grid smoothing is applied at plotting in the following figures.

3. Results

Figure 1 displays the global distribution of the wave activity in different seasons averaged during years of 2010–2013, with the left column for density and the right one for zonal wind. The focus of our study is on tropical regions (about 20°S–20°N). In these regions, we immediately notice a prominent three-peak longitudinal structure, with stronger wave activity over continents than oceans. A similar three-peak feature was reported at 400 km altitude in *Park et al.* [2014], but not in *Forbes et al.* [2016]. The choice of the perturbation parameter (RMS) and grid size might have an influence on results in the latter.

Outside the tropics over the Andes in South America, the wave activity enhances greatly around June solstice. Similar enhancements was observed at 400 km height and attributed to upward propagating mountain waves in this region [*Park et al.*, 2014]. Enhancements above about 50° latitudes at other longitudes and those over North America (high geomagnetic latitudes) are most likely related to auroral activities [*Park et al.*, 2014; *Forbes et al.*, 2016].

To have a closer look at the seasonal evolution of the longitudinal structure in the tropics, we extract GWs over 20°S–20°N latitudes and present the average in Figure 2. It reveals distinct longitudinal variation in all months, with three enhancements roughly around −70°, 10°, and 110° longitudes. Around solstices, an additional minor peak occurs near ±180° longitude in both the density and wind, with much smaller magnitude than the other three. It is interesting to note that the three major peaks shift gradually eastward from June to December, resembling the behavior of GWs in the stratosphere [*Jiang et al.*, 2004, Figure 4]. In general, the three-peak pattern in the density is less pronounced than in the wind. This is likely because total mass density perturbations depend not only on temperature perturbations, but also on the $[O]/[N_2]$ mixing ratio and transport by wind. These factors could be out of phase with each other, leading to a less clear pattern than that in the wind.

Figure 3 presents the zonally averaged wave activity at different latitudes in each month. It reveals a pronounced semiannual oscillation (SAO) at both tropical and middle latitudes, with maxima around solstices and deep minima around equinoxes. This SAO component resembles seasonal variations of GWs in the mesosphere [e.g., *Tsuda et al.*, 1994; *Fritts and Alexander*, 2003]. A less prominent annual oscillation (AO) is also visible in Figure 3, with wave activity maximizes around June solstice in the tropics (also seen in Figure 2). At middle latitudes, it exhibits strongest wave activity in local winter (June solstice in the southern hemisphere and December solstice in the northern hemisphere), which is similar to GWs in the mesosphere and lower thermosphere (MLT) region excited by winter jet streams [*Tsuda et al.*, 1994; *Fritts and Alexander*, 2003].

Figure 4 shows the global distribution of gravity waves in year 2010, when the solar flux level is low ($F_{10.7} \approx 70$ sfu). In comparison to Figure 1 where the average $F_{10.7}$ is around 110 sfu, the magnitude of the perturbations

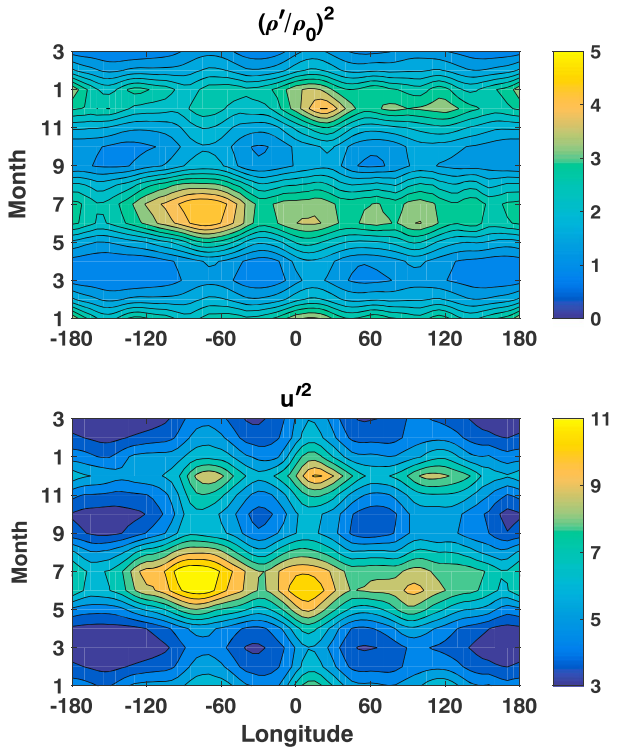

Figure 2. Longitude versus month distribution of GW variance in tropics averaged over 20°S–20°N latitudes. The month is repeated from January–March on the *y* axis to show activity around December solstice more completely. (top) Density, in units of 10^{-5}. (bottom) Zonal wind, in units of m^2/s^2.

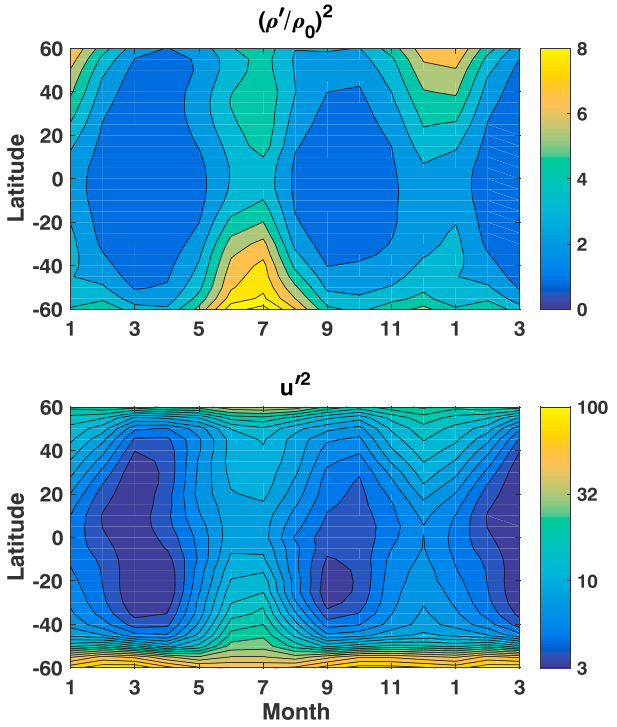

Figure 3. Seasonal variation of GW variance at different latitudes. January–March is repeated on the x axis to show activity around December solstice more completely. (top) Density, in units of 10^{-5}. (bottom) Zonal wind, in units of m^2/s^2.

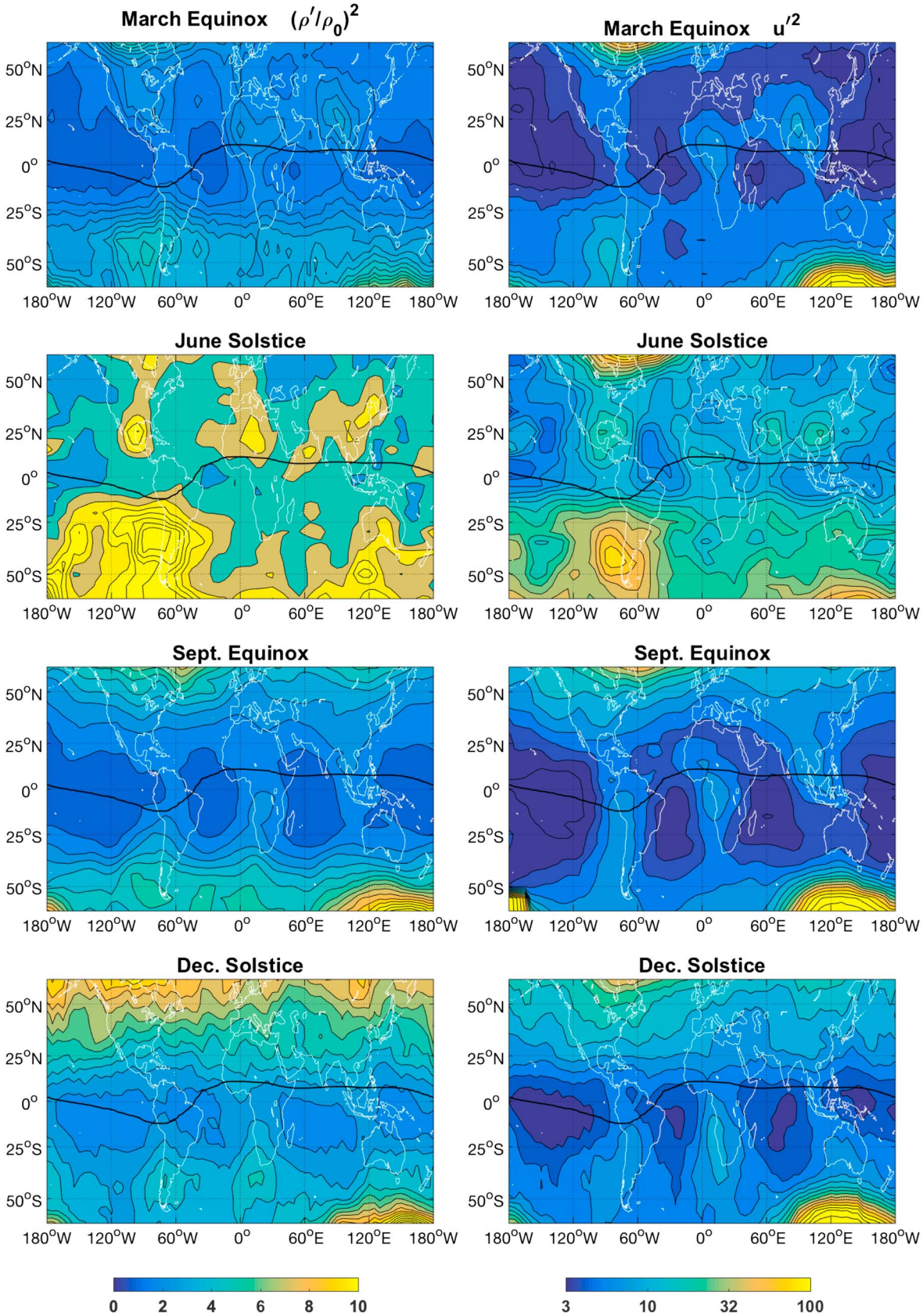

Figure 4. Same as for Figure 1 but in year 2010, when the average $F_{10.7}$ index was around 70 sfu.

increases considerably around June solstice, with the peak in central Pacific (near 180°W) also being more pronounced. These enhancements may indicate stronger GW activity at lower solar flux levels but could also potentially be year-to-year variation. Careful quantitative analysis with longer observations at the same pressure level is needed to clarify the solar cycle dependence.

4. Discussions

Medium-scale gravity wave activities in bottomside *F* region have been investigated using direct neutral density and wind measurements in the postsunset sector. Our analysis reveals consistent features in both the density and wind, suggesting the two are capturing signatures of the same GW perturbations. These perturbations show a pronounced three-peak longitudinal distribution, with stronger wave activity over land than ocean in the tropics. These wave activities strengthen around solstices and weaken around equinoxes. In the following, we discuss their implications on equatorial plasma bubble generation and possible wave sources.

As mentioned in the introduction, GWs in the bottomside *F* region are proposed to seed equatorial plasma bubbles [e.g., *Abdu et al.*, 2009, and references therein]. Figure 2 shows a strong longitude dependence of GW wave activity in the tropics, being enhanced in the Peruvian, African, and Western Pacific sectors in all seasons and also in central Pacific (±180°) around June solstice. These longitude sectors roughly overlap with those of high EPB occurrence [e.g., *Burke et al.*, 2004], hence lending a supporting sign to the GW-seeding hypothesis in terms of spatial distribution.

On the other hand, the climatological variations of GWs and EPBs are quite different. *Burke et al.* [2004] showed detailed climatology of EPBs occurrence rate, which is lowest around June solstice and highest around equinoxes at most longitudes except for the Peruvian sector, where EPBs maximize around December. In contrast, thermospheric GW activities minimize around equinoxes and maximize around June solstice (see Figure 2). In addition, they do not weaken toward solar minimum (see Figure 4), when there are very few EPBs. These almost opposite trends seem to cast doubt on a statistically positive correlation between GWs and EPBs. That is, stronger GW activity may not always lead to more EPBs, at least for GWs in this study with horizontal scales below 620 km. This implication is in line with the works of *Burke et al.* [2004], *Kudeki et al.* [2007], and *Yokoyama et al.* [2015], who found that instead of gravity waves, other factors like the magnetic declination, strong zonal winds, or vertical shear of zonal plasma drift can play more important roles in controlling EPB occurrence. Notably, the seasonal variation of the zonal wind in the evening sector fits perfectly to that of the EPB, with strongest wind around equinoxes, and weakest wind around June solstice [*Liu et al.*, 2016]. It is possible that GW seeding only accounts for the deviation from the declination-controlled pattern. To truly resolve the gravity wave and EPB relation, simultaneous neutral and plasma observations in the bottomside *F* region should be examined for a large number of EPBs.

Finally, we would like to briefly discuss possible generation sources for the bottomside medium-scale GWs in tropical regions. There are three potential sources: the auroral activity, the sunset solar terminator (ST), and the tropical deep convection. Since we use only measurements under quiet geomagnetic conditions, the auroral origin can almost be safely discarded. On the other hand, the sunset terminator is a stable wave source and can generate a spectrum of GWs varying with altitudes [*Somsikov*, 1987; *Bespalova et al.*, 2016]. At 200–300 km height, ST-generated GWs normally have horizontal scales over 1000 km. This renders the ST an unlikely source for GWs at scales of 155–620 km revealed in our study, hence leaving tropical deep convection the most promising one. *Vadas* [2007] has demonstrated that tropical deep convection can generate GWs that are capable of reaching the thermosphere ultimately. The resemblance of GWs global distribution in Figure 1 to the tropical topography and the distribution of water vapor and GWs in the stratosphere [*Hocke and Tsuda*, 2001] are consistent with this troposphere origin. However, since primary GWs generated by deep convection can hardly propagate directly to 250 km height, bottomside *F* region GWs are likely secondary GWs born from wave breaking of primary ones in the mesosphere and lower thermosphere (MLT) [*Vadas*, 2007]. The semiannual oscillation of the thermospheric GWs is also consistent with that of the MLT GWs [e.g., *Tsuda et al.*, 1994; *Fritts and Alexander*, 2003] and of the eddy diffusion coefficient (Kzz) [*Fukao et al.*, 1994], which represents gravity wave breaking in the MLT region.

To summarize, this study reveals a strong longitudinal dependence of the medium-scale gravity wave activity in bottomside *F* region. The global map and climatology obtained here provide new perspectives for investigating the occurrence of equatorial plasma bubbles and also for coupling between the lower and upper atmosphere via gravity waves.

Acknowledgments
We thank E. Doornbos for providing the GOCE data, which is accessible at https://earth.esa.int/web/guest/missions/esa-operational-missions/goce/goce-thermospheric-data. This work is supported by JSPS KAKENHI grants 15K05301 and 15H02135. The National Center for Atmospheric Research is supported by the U.S. National Science Foundation.

References

Abdu, M., E. A. Kherani, I. S. Batista, E. R. de Paular, D. Fritts, and J. H. A. Sobral (2009), Gravity wave initiation of equatorial spread *F*/plasma bubble irregularities based on obsevational data from the SpreadFEx campaign, *Ann. Geophys.*, *67*, 2607–2622.

Bespalova, A. V., A. K. Fedorenko, O. K. Cheremnykh, and I. T. Zhuk (2016), Satellite observations of wave disturbances caused by moving solar terminator, *J. Atmos. Sol. Terr. Phys.*, *140*, 79–85, doi:10.1016/j.jastp.2016.02.012.

Burke, W. J., L. C. Gentile, C. Y. Huang, C. E. Valladares, and S. Y. Su (2004), Longitudinal variability of equatorial plasma bubbles observed by DMSP and ROCSAT-1, *J. Geophys. Res.*, *109*, A12301, doi:10.1029/2004JA010583.

Doornbos, E., S. L. Bruinsma, B. Fritsche, G. Koppenwallner, P. Visser, J. van den IJssel, and J. de Teixeira Encarnacao (2013), Air density and wind retrieval using GOCE data, *Final Rep. ESA AO/1-6367/10/NL/AF*, European Space Agency, TU Delft, Netherlands.

Forbes, J. M., S. L. Bruinsma, E. Doornbos, and X. Zhang (2016), Gravity wave-induced variability of the middle thermosphere, *J. Geophys. Res. Space Physics*, *121*, 6914–6923, doi:10.1002/2016JA022923.

Fritts, D. C., and M. J. Alexander (2003), Gravity wave dynamics and effects in the middle atmosphere, *Rev. Geophys.*, *41*(1), 1003, doi:10.1029/2001RG000106.

Fritts, D. C., et al. (2008), Gravity wave and tidal influences on equatorial spread *F* based on observations during the Spread *F* Experiment (SpreadFEx), *Ann. Geophys.*, *26*, 3235–3252.

Fukao, S., M. D. Yamanaka, N. Ao, W. K. Hocking, T. Sato, M. Yamamoto, N. Nakamura, T. Tsuda, and S. Kato (1994), Seasonal variability of vertical eddy diffusivity in the middle atmosphere: 1. Three-year observations by the middle and upper atmosphere radar, *J. Geophys. Res.*, *99*, 18,973–18,987, doi:10.1029/94JD00911.

Hei, H., T. Tsuda, and T. Hirooka (2008), Characteristics of atmospheric gravity wave activity in the polar regions revealed by GPS radio occultation data with CHAMP, *J. Geophys. Res.*, *113*, D04107, doi:10.1029/2007JD008938.

Hocke, K., and T. Tsuda (2001), Gravity waves and ionospheric irregularities over tropical convection zones observed by GPS/MET Radio Occultation, *Geophys. Res. Lett.*, *28*, 2815–2818, doi:10.1029/2001GL013076.

Jacobi, C. (2014), Long-term trends and decadal variability of upper mesosphere/lower thermosphere gravity waves at midlatitudes, *J. Atmos. Sol. Terr. Phys.*, *118*, 90–95, doi:10.1016/j.jastp.2013.05.009.

Jiang, J., B. Wang, K. Goya, K. Hocke, S. Eckermann, J. Ma, D. Wu, and W. Read (2004), Geographical distribution and interseasonal variability of tropical deep convection: UARS MLS observations and analyses, *J. Geophys. Res.*, *109*, D03111, doi:10.1029/2003JD003756.

Kudeki, E., A. Akgiray, M. Milla, J. L. Chau, and D. L. Hysell (2007), Equatorial spread-*F* initiation: Post-sunset vortex, thermospheric winds, gravity waves, *J. Atmos. Sol. Terr. Phys.*, *69*, 2416–2427, doi:10.1016/j.jastp.2007.04.012.

Liu, H., E. Doornbos, and J. Nakashima (2016), Thermospheric wind observed by GOCE: Wind jets and seasonal variations, *J. Geophys. Res. Space Physics*, *121*, 6901–6913, doi:10.1002/2016JA022938.

Park, J., H. Lühr, C. Lee, Y. H Kim, G. Jee, and J.-H. Kim (2014), A climatology of medium-scale gravity wave activity in the midlatitude/low-latitude daytime upper thermosphere as observed by CHAMP, *J. Geophys. Res. Space Physics*, *119*, 2187–2196, doi:10.1002/2013JA019705.

Rebhan, H., M. Aguirre, and J. Johannessen (2000), The Gravity Field and Steady-State Ocean Circulation Explorer mission—GOCE, *ESA Earth Obs. Q.*, *66*, 6–11.

Somsikov, V. M. (1987), A spherical model of wave generation in the atmosphere by the solar terminator, *J. Atmos. Terr. Phys.*, *49*, 433–438.

Tsuda, T., Y. Murayama, T. Nakamura, R. A. Vincent, A. H. Manson, C. E. Meek, and R. L. Wilson (1994), Variations of the gravity wave characteristics with height, season and latitude revealed by comparative observations, *J. Atmos. Terr. Phys.*, *56*, 555–568, doi:10.1016/0021-9169(94)90097-3.

Vadas, S. L. (2007), Horizontal and vertical propagation and dissipation of gravity waves in the thermosphere from lower atmospheric and thermospheric sources, *J. Geophys. Res.*, *112*, A06305, doi:10.1029/2006JA011845.

Watanabe, S., and H. Oya (1986), Occurrence characteristics of low latitude ionosphere irregularities observed by impedance probe on board the Hinotori satellite, *J. Geomagn. Geoelectr.*, *38*, 125–149.

Yokoyama, T., H. Jin, and H. Shinagawa (2015), West wall structuring of equatorial plasma bubbles simulated by three-dimensional HIRB model, *J. Geophys. Res. Space Physics*, *120*, 8810–8816, doi:10.1002/2015JA021799.